GDCh **Communications** Angewandte International Edition Chemie www.angewandte.org

Oxygen Reduction Reaction **Hot Paper**

How to cite: *Angew. Chem. Int. Ed.* **2022,** *61,* e202116727
International Edition: doi.org/10.1002/anie.202116727
German Edition: doi.org/10.1002/ange.202116727

Cylindrical C_{96} Fullertubes: A Highly Active Metal-Free O_2-Reduction Electrocatalyst

Mohamed Fathi Sanad, Hannah M. Franklin, Basant A. Ali, Alain R. Puente Santiago, Aruna N. Nair, Venkata S. N. Chava, Olivia Fernandez-Delgado, Nageh K. Allam, Steven Stevenson,* Sreeprasad T. Sreenivasan,* and Luis Echegoyen**

Abstract: A new isolation protocol was recently reported for highly purified metallic Fullertubes D_{5h}-C_{90}, D_{3d}-C_{96}, and D_{5d}-C_{100}, which exhibit unique electronic features. Here, we report the oxygen reduction electrocatalytic behavior of C_{60}, C_{70} (spheroidal fullerenes), and C_{90}, C_{96}, and C_{100} (tubular fullerenes) using a combination of experimental and theoretical approaches. C_{96} (a metal-free catalyst) displayed remarkable oxygen reduction reaction (ORR) activity, with an onset potential of 0.85 V and a halfway potential of 0.75 V, which are close to the state-of-the-art Pt/C benchmark catalyst values. We achieved an excellent power density of $0.75\ \mathrm{W\,cm^{-2}}$ using C_{96} as a modified cathode in a proton-exchange membrane fuel cell, comparable to other recently reported efficient metal-free catalysts. Combined band structure (experimentally calculated) and free-energy (DFT) investigations show that both favorable energy-level alignment active catalytic sites on the carbon cage are responsible for the superior activity of C_{96}.

Fuel cells represent a desirable solution to improve the continuously rising energy demands and the environmental impact of traditional energy sources.[1] Fuel cells directly generate electricity by electrochemically reducing oxygen and oxidizing hydrogen with water as the only byproduct.[2] Currently, platinum (Pt)-group metal-based catalysts (PGM) are the most active catalysts for the oxygen reduction reaction (ORR). Typical Pt/C-based electrocatalysts represent about half the cost (projected by the US Department of Energy) of an automotive fuel cell stack, which hinders fuel cell technology commercialization.[3] The high price of conventional platinum nanoparticles-based catalysts and the large consumption of Pt in fuel cells is a consequence of the sluggish ORR kinetics and the low atomic utilization capability on a per Pt atom basis since only a tiny portion of the Pt atoms on the particle surface area are associated with electrocatalysis. To enhance the large-scale application of fuel-cell systems, cost-feasible and efficient non-precious metal ORR electrocatalysts must be developed as replacements for the scarce Pt-based catalysts. Many efforts have been devoted to discovering efficient, stable, and inexpensive options to replace Pt.[4] Heteroatom-doped nanostructured carbon materials, heterostructures, and metal–organic frameworks are significant platforms for metal-free electrocatalysts for oxygen reduction reactions because of their unique electronic properties.[5] Despite some remarkable accomplishments attained by the thoughtful adoption of suitable precursors and the optimization of nanostructuring processes, the ORR performance of metal-free catalysts is still inferior to those of the state-of-the-art Pt/C catalysts in terms of its half-wave potential.[6] These metal-free electrocatalysts are not structurally well characterized and often contain impurities.[6c] These drawbacks decrease the reproducibility and hinder the practical applications of the current metal-free electrocatalysts.[2,7] Herein, we studied the feasibility of using fullertubes as metal-free oxygen reduction catalysts using a combination of density functional theory (DFT) and electrocatalytic methods. Fullertubes are characterized by two fullerene endcaps and a tubular midsection composed of a single graphene layer. Fullertube endcaps include the following two structures: a) Half of a C_{60} with a pentagon-based symmetry axis and b) half of a C_{60} with a hexagon-based symmetry axis.[10]

Figure 1a illustrates the ball-and-stick representations of C_{60}, C_{70}, C_{90}, C_{96}, and C_{100}. The compositions of C_{60}, C_{70}, C_{90}, C_{96}, and C_{100} were confirmed using both HPLC and MALDI-TOF, comparing simulated and experimental spectra (Figures S1 and S2). Figure S3 shows the Raman spectrum of the fullerenes and fullertubes studied. Typically, the Raman peak near $1468\ \mathrm{cm^{-1}}$ describes the benzoic ring

---

[*] M. F. Sanad
Department of Chemistry and Biochemistry and Environmental Sciences and Engineering, The University of Texas at El Paso,
500 W. University Avenue, El Paso, TX 79968 (USA)

H. M. Franklin, Prof. S. Stevenson
Department of Chemistry, Purdue University,
Fort Wayne, IN 46805 (USA)
E-mail: stevenss@pfw.edu

B. A. Ali, Prof. N. K. Allam
Energy Materials Laboratory, School of Sciences and Engineering,
The American University in Cairo,
New Cairo 11835 (Egypt)
E-mail: nageh.allam@aucegypt.edu

Dr. A. R. Puente Santiago, A. N. Nair, Dr. V. S. N. Chava,
Dr. O. Fernandez-Delgado, Dr. S. T. Sreenivasan, Prof. L. Echegoyen
Department of Chemistry and Biochemistry,
The University of Texas at El Paso,
500 W. University Avenue, El Paso, TX 79968 (USA)
E-mail: sreenivasan@utep.edu
echegoyen@utep.edu

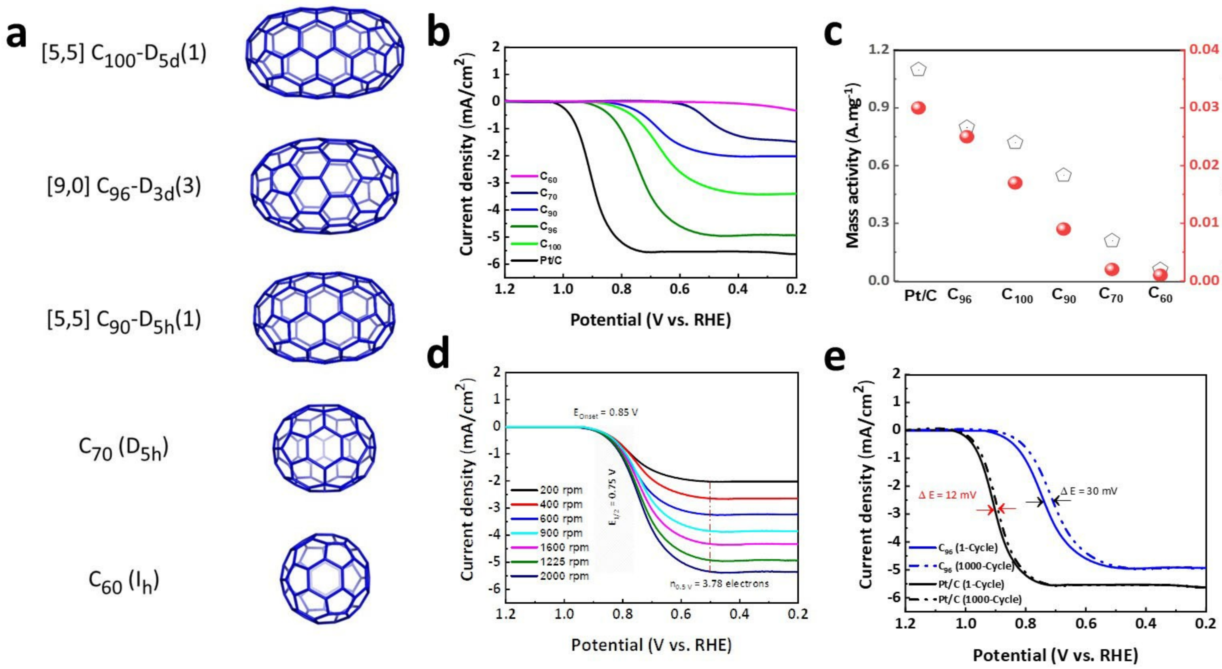

Figure 1. a) Structure representation of the C_{60}, C_{70}, C_{90}, C_{96}, and C_{100}. b) Linear sweep voltammetry (LSV) of C_{60}, C_{70}, C_{90}, C_{96}, and C_{100} compared to Pt/C (electrode-rotating speed, 1600 r.p.m.). c) Specific activity and mass activity of the C_{60}, C_{70}, C_{90}, C_{96}, and C_{100} molecular catalysts. d) O_2 Rotating disk electrode plots of C_{96} in oxygen-saturated 0.1 M KOH solution at rotation speeds ranging from 200 to 2000 r.p.m and a scan rate of 10 mV s^{-1}. e) Polarization curves of C_{96} and Pt/C catalysts before (solid) and after (dotted) 1000 ORR cycle.

breath for spherical C_{60}, while the 1563 cm^{-1}peak is related to a fingerprint C_{70} Raman peak.[8] Additionally, the Raman feature most generally employed to characterize Fullertubes is the G- band at ≈1580–1600 cm^{-1}, a vibrational mode prevalent for sp^2 carbons and a characteristic mode exclusive for all C_{90}, C_{96}, and C_{100} fullertubes. Fullertubes have a rolled graphene tubular belt region of 6,6 ring junctions less active than the more reactive 5,6 ring junctions located at the endcaps.

The oxygen reduction electrochemical performance of the fullerenes and fullertubes was investigated using linear sweep voltammetry at 1600 rpm in O_2 saturated 0.1 M KOH alkaline medium. Figure 1b depicts the rotating disk electrode voltammograms of a glassy carbon electrode loaded with the ink of C_{60} I_h, C_{70} D_{5h}, C_{90} D_{5h} (1), C_{96} D_{3d} (1), and C_{100}-D_{5d} (1). When the electrode potential was swept negatively, the nonzero current started to rise, indicating oxygen reduction catalyzed by these fullerenes. The onset potential (E_{onset}) was found to increase in the order of C_{60} (+0.40 V) & ek; $<C_{70}$ (+0.60 V) $<C_{90}$ (+0.80 V) $<C_{100}$ (+0.82 V) $<C_{96}$ (+0.85 V). C_{96} surpassed other fullertubes and fullerenes with an onset potential of 0.85 V and a halfway potential of 0.75 V versus a reversible hydrogen electrode (RHE). The catalyst achieved 0.73 A/mg mass activity, a very significant and promising value for a metal-free electrocatalyst. The same trend was observed for the specific activity of C_{96} (0.027 mA cm^{-2}), which is in the range of the state-of-the-art of recently reported values for some metal-free catalysts (Figure 1c).[9] The Double-layer capacitance (C_{dl}) is related to the electrochemical surface area (ECSA). It can be calculated using cyclic voltammetry by sweeping the voltage in the non-faradaic potential range at different scan rates, as shown in Figure S4. The double-layer capacitance C_{dl} of C_{96} was found to be 1.02 mF cm^{-2}, which is larger than for the other fullerenes and fullertubes, indicating that the C_{96} interface has a higher ability to store charges (Figure S4). The dynamic oxygen reduction reaction (ORR) properties at different electrode rotation rates were studied for C_{96} in detail using a rotating disk electrode (RDE) set up to probe the kinetics of the interfacial redox reactions on both catalytic surfaces under non diffusion conditions (Figure 1d). C_{96} displayed excellent electrocatalytic activity toward ORR. The linearity of the Koutecky–Levich (K–L) plots for C_{96} indicates first-order reaction kinetics as a function of the concentration of dissolved oxygen. The K–L plots also revealed that C_{96} fullertubes show a superior catalytic activity, which is close to that for Pt/C under dynamic environments.[10] The average value of n (the number of electrons) was estimated to be 3.76 electrons transferred per oxygen molecule during the electrocatalytic reaction, a fundamental descriptor of the ORR kinetic efficiency (Figure S5). This also indicates that some types of intermediates might be formed other than water. The long-term durability of C_{96} and Pt/C were also assessed. Notably, the half-wave potential ($E_{1/2}$) for C_{96} after 1000 cycles exhibited a 30 mV shift compared to 12 mV observed for commercial Pt/C (Figure 1e). Electrocatalyst band structure is an essential factor that affects the ORR capability.[11] As shown in Figure 2a and Figure S6, the valence band of C_{96} is closer to that of the standard water splitting and oxygen

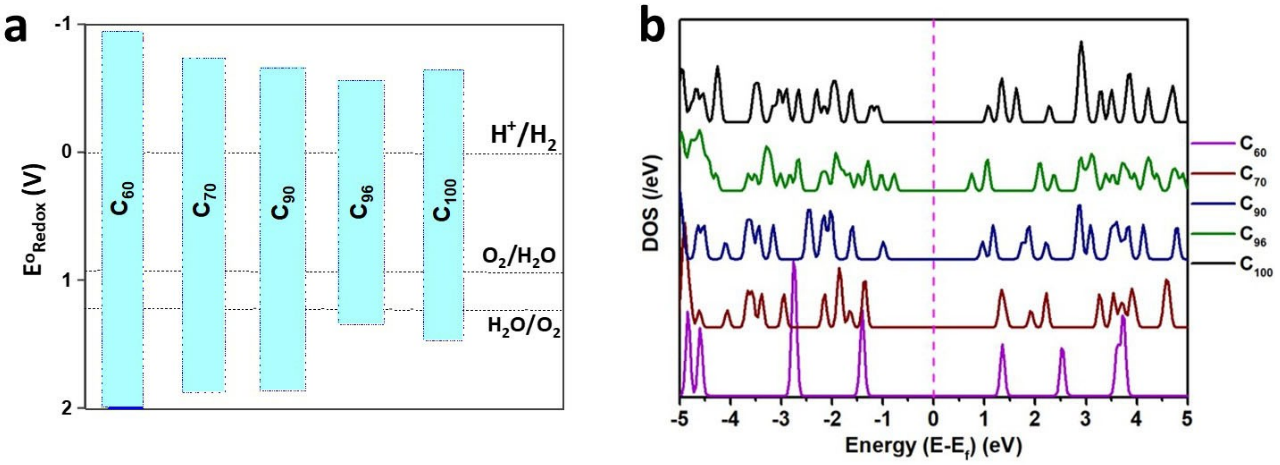

Figure 2. a) Experimental band structure of C_{60}, C_{70}, C_{90}, C_{96}, and C_{100}. b) Density of states (DOS) of C_{60}, C_{70}, C_{90}, C_{96}, and C_{100}.

reduction reaction standard potentials, which indicates the potential capability of C_{96} to reduce oxygen.

The electronic properties of the fullerenes and fullertubes were further investigated using Gaussian 16 with the use of the B3LYP method and the 6-31G basis set. The results were visualized and analyzed using GaussSum. The study included the optimization for C_{60} I_h, C_{70} D_{5h}, C_{90} D_{5h} (1), C_{96} D_{3d} (1), and C_{100}-D_{5d} (1). The calculations provide insights about the band gap energy of the fullerenes, as illustrated in Figure 2b. It can be observed that C_{100} has band gap energy (2.2 eV) considerably lower than those of C_{70} (2.48 eV) and C_{60} (2.56) and higher than that of C_{90} (1.7 eV) and C_{96} (1.15 eV). The calculated band gap energies are close to the experimental values for C_{60}–C_{96} but not for $C_{100,}$ which shows a bit higher band gap energy. The density of states (DOS) presented in Figure 2b shows that C_{60} exhibits the highest DOS in the non-occupied states. In contrast, C_{96} and C_{100} show the highest DOS in the occupied states, providing insights about the reactivity of C_{100} in the ground state. The electronic Mulliken charge calculations showed that C_{60} has zero charges on the carbon skeleton. At the same time, all higher fullerenes possess electronically non-equivalent carbon sites (i.e., carbon atoms with non-equal charges or electrical fields) with different charges in the range of 0.058 and −0.041, as shown in Figures S7.

Our density of states calculations show a high density of states near the Fermi level in the case of C_{90}, $C_{96,}$ and $C_{100,}$ supporting the high electrocatalytic activity of the fullertubes as shown in Figure 2b.[12] DFT was also used to calculate the free energy of the oxygen reduction reaction intermediates over the C_{96} and Pt/C catalysts. The adsorption free energies were computed assuming a low oxygen coverage in both cases. As shown in Figure S8, adsorption energy calculations of oxygen species over the fullerenes and fullertubes shows that C_{96} compounds have three different types of active sites with acceptable energy values.

Our DFT calculations showed a good agreement with the experimental results. In detail, a significant reduction of the Gibbs free energies for the O*, OH*, and OOH* intermediate catalytic species was observed (Figure S9). The specific active sites are shown in Figure S8, which match with NBO charge distribution in Figure S10. Gibbs free energy and ORR reaction intermediates over both C_{96} and Pt/C are shown in Figure S9. Free energy calculations show that the limiting elementary step for the oxygen reduction reaction (ORR) is $OH_{ads,}$ which has a small energy barrier for C_{96}, which firmly confirms its more favorable adsorption to the C_{96} surfaces.

Figures S10 show the natural bond charge distribution over the ball and stick representation of the isolated C_{100} and C_{96} crystals. Their high charge asymmetry through the whole skeleton creates potentially active sites for ORR. In the case of $C_{96,}$ there are three different negatively charged active sites compared to only one position on C_{100}. NBO charge distributions also show that C_{96} is characterized by high electron density over the endcaps, suggesting that the endcaps are the most active sites for the ORR. NBO charge distributions for C_{60}, $C_{70,}$ and C_{90} are also shown in Figure S11.

The fuel cell used is shown in Figure 3a and features graphite plates with gas flow channels and an active area of 6 cm^2. Pure hydrogen and pure oxygen gases were supplied to the anode and cathode sides of the cell, respectively. The cell was allowed to stabilize for two h before recording polarization curves. Pt/C and C_{96} loading were 0.5 mg/cm^2. Polarization curves were recorded using a CHI potentiostat. Pt/C was used for the hydrogen oxidation reaction (HOR), and C_{96} was used as a modified ORR catalyst. Figure 3b shows the results of the fuel cell tests using a C_{96} catalyst and a commercial Pt/C catalyst (40 wt % Pt on carbon) at the cathode for comparison. For C_{96}, the fuel cell produced 0.75 W cm^{-2}, which is reasonably close to the value for Pt/C (0.9 W cm^{-2}). Figure 3c shows a column chart comparing the power density achieved using C_{96} as an ORR cathode with other reported highly active metal-free catalysts. C_{96} exhibited better performance than other metal-free catalysts such as g-C_3N_4 with a carbon nanofiber hybrid,[13] amorphous N-doped carbon film,[14] N, S-doped mesoporous carbon,[15] and carbon nanotubes/heteroatom-doped carbon core-sheath nanostructures metal-free catalysts (Figure 3c).[16] C_{96}

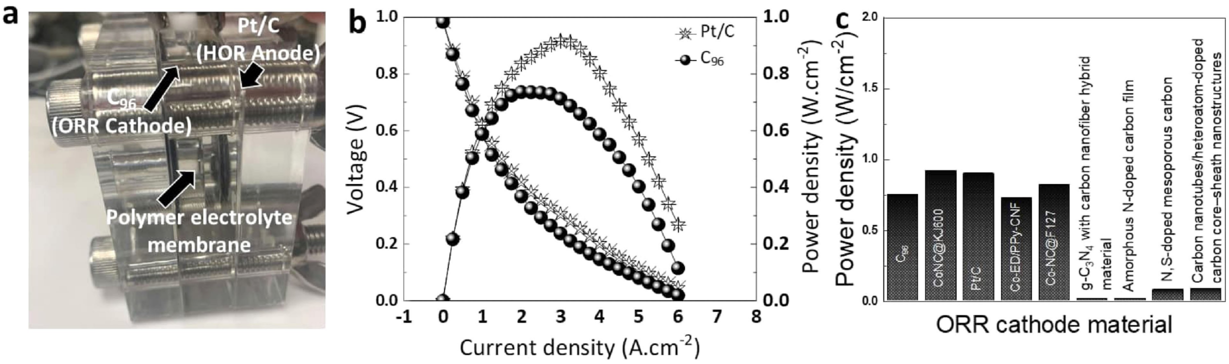

Figure 3. a) The fuel cell setup: Pt/C used as anode and C_{96} used as cathode. b) Polarization curves and power density curves for the polymer membrane fuel cell using C_{96} as ORR Cathode and Pt/C as HOR anode. c) Comparison of the power density achieved by C_{96} with the highest reported value for metal free ORR catalysts.

performs similarly to some metal-based electrocatalysts such as Co-NC@F127, Co-ED/PPy-CNF, and NC@KJ600 (Figure 3c).[17]

The high performance of C_{96} establishes the superiority of C_{96} fullertubes as metal-free catalysts and a new alternative to other reported metal-free catalysts. The other Fullerenes and Fullerutbes followed the same ORR performance trend in power density in the fuel cells, as shown in Figure S12.

In conclusion, we have introduced highly purified forms of fullertube nanostructures, synthesized using the arcing method, as metal-free molecular catalysts. The band structure of different types of fullertubes was investigated using both theoretical and experimental approaches. Based on the band alignment (i.e., HOMO–LUMO levels), we found that C_{96} is a good oxygen reduction molecular catalyst. Electrochemical measurements confirmed that C_{96}, compared to C_{60}, C_{70}, $C_{90,}$ and C_{100}, shows a high catalytic activity toward ORR with good stability after 1000 cycles. C_{96} achieved oxygen reduction with a notable onset potential of 0.85 V and a halfway potential of 0.75 V, close to the values for the Pt/C benchmark catalyst ($E_{\mathrm{onset}} = 0.9$ V). A high fuel cell power density of 0.75 W cm^{-2}, achieved by employing C_{96} as a modified cathode in a proton exchange membrane fuel cell, suggests the superiority of these materials when compared to Other recently reported metal-free catalysts. Considering the ORR performance, fuel cell power density, and compound purity, C_{96} fullertubes are very promising oxygen reduction electrocatalysts. One drawback is the production yields of fullertubes. The challenge is to improve the synthesis methods to produce the fullertubes at higher yields which should be feasible. As opposed to PGMs, the fullertubes constituent elements carbon and hydrogen are not limited by natural abundance, so higher yields should be possible via new synthetic methods.

Acknowledgements

L.E. wants to thank the NSF for the generous support of this work under CHE-1801317. The Robert A. Welch Foundation is also gratefully acknowledged for an endowed chair to L.E. (grant AH-0033). S.T.S. acknowledges support from UTEP start-up grant and UT STARs award. S.T.S. acknowledges the partial support from DOE under grant #DE-FE0031908. S.T.S also acknowledge the partial support from a seed grant through Nanotechnology collaborative Infrastructure (NCI)-Southwest program supported in part by NSF program NNCI-ECCS-1542160. S.S. acknowledges funding from NSF RUI 1856461. N.K.A. acknowledges the financial support from the Arab-German Young Academy of Sciences and Humanities (AGYA).

Conflict of Interest

The authors declare no conflict of interest.

Data Availability Statement

The data that support the findings of this study are available in the supplementary material of this article.

Keywords: Band Alignment · C_{96} · Electrocatalysis · Fullerenes · Molecular Catalysis · Oxygen Reduction Reaction

---

[1] D. A. Cullen, K. C. Neyerlin, R. K. Ahluwalia, R. Mukundan, K. L. More, R. L. Borup, A. Z. Weber, D. J. Myers, A. Kusoglu, *Nat. Energy* **2021**, *6*, 462–474.
[2] K. Kodama, T. Nagai, A. Kuwaki, R. Jinnouchi, Y. Morimoto, *Nat. Nanotechnol.* **2021**, *16*, 140–147.
[3] U. Martinez, S. Komini Babu, E. F. Holby, H. T. Chung, X. Yin, P. Zelenay, *Adv. Mater.* **2019**, *31*, 1806545.
[4] Z. Xia, L. An, P. Chen, D. Xia, *Adv. Energy Mater.* **2016**, *6*, 1600458.
[5] a) M. Guo, M. Xu, Y. Qu, C. Hu, P. Yan, T. T. Isimjan, X. Yang, *Appl. Catal. B* **2021**, *297*, 120415; b) L. Yang, J. Shui, L. Du, Y. Shao, J. Liu, L. Dai, Z. Hu, *Adv. Mater.* **2019**, *31*, 1804799.
[6] a) W. Wei, H. Liang, K. Parvez, X. Zhuang, X. Feng, K. Müllen, *Angew. Chem. Int. Ed.* **2014**, *53*, 1570–1574; *Angew.*

Chem. **2014**, *126*, 1596–1600; b) Z. Jiang, Z.-j. Jiang, X. Tian, W. Chen, *J. Mater. Chem. A* **2014**, *2*, 441–450; c) L. Wang, A. Ambrosi, M. Pumera, *Angew. Chem. Int. Ed.* **2013**, *52*, 13818–13821; *Angew. Chem.* **2013**, *125*, 14063–14066.

[7] a) J. Zhang, H. Yang, B. Liu, *Adv. Energy Mater.* **2021**, *11*, 2002473; b) G. Ramos-Sanchez, S. Praserthdam, F. Godinez-Salomon, C. Barker, M. Moerbe, H. A. Calderon, L. A. Lartundo, M. A. Leyva, O. Solorza-Feria, P. B. Balbuena, *Phys. Chem. Chem. Phys.* **2015**, *17*, 28286–28297.

[8] S. Stevenson, X. Liu, D. M. Sublett, R. M. Koenig, T. L. Seeler, K. R. Tepper, H. M. Franklin, X. Wang, R. Huang, X. Feng, K. Cover, D. Troya, N. Shanaiah, R. J. Bodnar, H. C. Dorn, *J. Am. Chem. Soc.* **2021**, *143*, 4593–4599.

[9] G. W. Sievers, A. W. Jensen, J. Quinson, A. Zana, F. Bizzotto, M. Oezaslan, A. Dworzak, J. J. K. Kirkensgaard, T. E. L. Smitshuysen, S. Kadkhodazadeh, M. Juelsholt, K. M. Ø. Jensen, K. Anklam, H. Wan, J. Schäfer, K. Čépe, M. Escudero-Escribano, J. Rossmeisl, A. Quade, V. Brüser, M. Arenz, *Nat. Mater.* **2021**, *20*, 208–213.

[10] C. C. Hou, L. Zou, L. Sun, K. Zhang, Z. Liu, Y. Li, C. Li, R. Zou, J. Yu, Q. Xu, *Angew. Chem. Int. Ed.* **2020**, *59*, 7384–7389; *Angew. Chem.* **2020**, *132*, 7454–7459.

[11] a) C. Chen, X.-T. Wang, J.-H. Zhong, J.-L. Liu, G. Waterhouse, Z.-Q. Liu, *Angew. Chem. Int. Ed.* **2021**, *60*, 22043–22050; *Angew. Chem.* **2021**, *133*, 22214–22221; b) M. F. Sanad, V. S. N. Chava, A. E. Shalan, L. G. Enriquez, T. Zheng, S. Pilla, S. T. Sreenivasan, *ACS Appl. Mater. Interfaces* **2021**, *13*, 40731–40741.

[12] B. Lu, T. J. Smart, D. Qin, J. E. Lu, N. Wang, L. Chen, Y. Peng, Y. Ping, S. Chen, *Chem. Mater.* **2017**, *29*, 5617–5628.

[13] O.-H. Kim, Y.-H. Cho, D. Y. Chung, M. J. Kim, J. M. Yoo, J. E. Park, H. Choe, Y.-E. Sung, *Sci. Rep.* **2015**, *5*, 8376.

[14] J. Chen, X. Wang, X. Cui, G. Yang, W. Zheng, *Chem. Commun.* **2014**, *50*, 557–559.

[15] Y. Qiu, J. Huo, F. Jia, B. H. Shanks, W. Li, *J. Mater. Chem. A* **2016**, *4*, 83–95.

[16] Y. J. Sa, C. Park, H. Y. Jeong, S.-H. Park, Z. Lee, K. T. Kim, G.-G. Park, S. H. Joo, *Angew. Chem. Int. Ed.* **2014**, *53*, 4102–4106; *Angew. Chem.* **2014**, *126*, 4186–4190.

[17] R. Wang, P. Zhang, Y. Wang, Y. Wang, K. Zaghib, Z. Zhou, *Prog. Nat. Sci.* **2020**, *30*, 855–860.

Manuscript received: December 7, 2021
Accepted manuscript online: March 7, 2022
Version of record online: March 23, 2022